(Received 2 February 2024, Accepted 9 March 2024, Scheduled 24 March 2024)

UHF-Band Solid Sensor Based on Tweaking Electric Field Coupled Resonator for Material Characterization

Syah Alam[1,*], Indra Surjati[1], Lydia Sari[1], Yuli K. Ningsih[1], Munanda Y. Fathanah[1], Yessi K. Gultom[1], Ghathfan Daffin[1], Teguh Firmansyah[2], and Zahriladha Zakaria[3]

[1]*Department of Electrical Engineering, Universitas Trisakti, Grogol, DKI Jakarta, Indonesia*
[2]*Department of Electrical Engineering, Universitas Sultan Ageng Tirtayasa, Banten, West Jakarta, Indonesia*
[3]*Faculty of Electronic and Computer Technology and Engineering, Universiti Teknikal Malaysia Melaka (UTeM), Malaysia*

ABSTRACT: This paper proposes a UHF-band microwave sensor for solid material detection based on a tweaking electric field coupled (ELC) resonator. The microwave sensor operates at a low resonant frequency of 0.82 GHz to characterize solid materials with a permittivity range of 1–9.8. The location of the sensing area is determined based on the surface of the resonator with the highest electric field. The permittivity of the sample is determined based on perturbation theory by observing the frequency shift relative to changes in the permittivity of the sample placed in the sensing area of the proposed sensor. From the measurement process, the proposed sensor has a normalized sensitivity (NS) of 1.49%, frequency detection resolution (FDR) of 0.012 GHz, and an average accuracy of 96.72%. This work has a significant contribution and can be recommended for several applications including the pharmaceutical, biomedical, and materials industries.

1. INTRODUCTION

Material characterization plays an important role for several applications such as the pharmaceutical, biomedical, and materials industries [1, 2]. Material characterization is very useful for knowing the ability and interaction of the material with changes in the surroundings, such as permittivity [3, 4]. Permittivity is a parameter that shows the interaction between a material and an electric field. One solution for detecting the permittivity of materials is a microwave sensor which has advantages including low cost, compact design, and high accuracy [5, 6]. The permittivity of the material is determined based on perturbation theory where the sample is placed in the sensing area of the sensor [7, 8]. The sensing area is determined based on the highest electric field on the surface of the resonator. The interaction between the sensor and the material causes the resonance frequency to change. Several previous works proposed microwave sensors for characterization of solid [9, 10], liquid [11, 12], and thickness materials. Generally, microwave sensors are proposed to operate at high frequencies in the GHz range [13, 14]. The application of high frequency microwave sensors provides advantages including compact design and high accuracy. Nevertheless, it has limited resolution when it comes to detecting small objects or distinguishing between closely spaced objects. Another limitation is interference from high environmental effects which can lead to inaccurate measurements. In addition, high frequency microwave sensors may require high power consumption and be expensive to implement infield practice. Therefore, low frequency microwave sensors can be proposed as a solution to produce sensors with low cost, low power consumption, and low interference from environmental effect so that they can be used for material characterization with precise and accurate measurements.

Previous work [15] proposed an Square split-ring resonator (SSRR)-based microwave sensor with a spurline operating at a resonant frequency of 2.2 GHz to detect the permittivity of solid materials in the range 1–4.4. Furthermore, [16] proposed a microwave sensor operating at dual frequencies of 9.54 GHz and 12.45 GHz to characterize solid materials with a permittivity range of 1–12.85. Furthermore, a microwave sensor based on a dual U-shaped resonator operating at resonant frequencies of 1.21 GHz and 2.1 GHz has been proposed for permittivity detection of solid materials [17]. Microwave sensors have also been proposed for permittivity detection of liquids. Another work proposed a microwave sensor using a substrate integrated waveguide (SIW) for permittivity detection of liquids with a resonance frequency range of 2.27 GHz–5.81 GHz [18, 19]. However, the normalized sensitivity obtained is still low. Another limitation is that the resonant frequency used is a high frequency with a range of 1–12 GHz, so it has the potential to be influenced by environmental interference and requires high consumption power. Therefore, microwave sensors which operate at low frequencies are needed to reduce interference from the environment with low power consumption.

This work proposes a microwave sensor operating at low frequencies that has high performance. The proposed sensor is based on a tweaking electric field coupled (ELC) resonator operating at a resonant frequency of 0.82 GHz. The application of the ELC resonator aims to increase the concentration of the electric field so that the sensor is more sensitive. The main contribution of this work is to produce a microwave sensor for permittivity detection of materials operating at low frequencies with high sensitivity and low interference with environmental

* Corresponding author: Syah Alam (syah.alam@trisakti.ac.id).

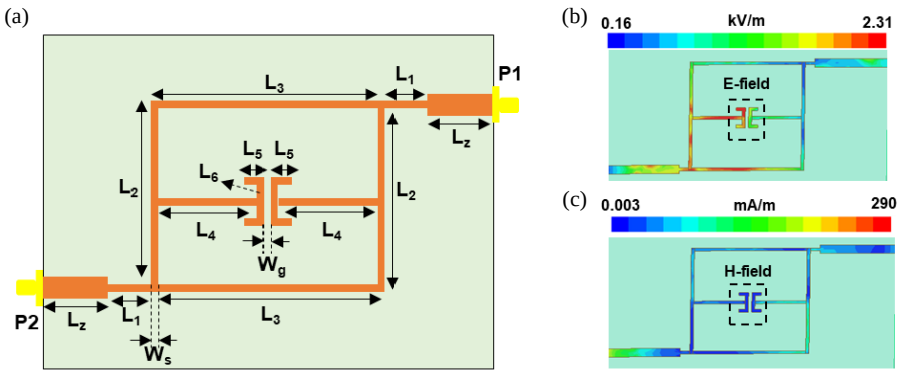

FIGURE 1. (a) Structure of proposed resonator, (b) E-field concentration at $f_r = 0.88$ GHz, (c) H-field concentration at $f_r = 0.88$ GHz.

effect so that it can be recommended for several applications such as pharmaceutical, biomedical, and materials industries.

2. WORKING PRINCIPLES OF PROPOSED SENSOR

The proposed microwave sensor is designed based on an ELC resonator with two ports using FR-4 with a permittivity of 4.3, a thickness of 1.6 mm, and a tan δ of 0.0265. The structure of the tweaking ELC resonator consists of an inductive arm separated by a gap in the middle of the resonator which is connected to port 1 and port 2 using a microstrip line as shown in Fig. 1(a). The overall dimensions of the ELC resonator are shown in Table 1. Furthermore, the electric field and magnetic field concentrations of the ELC resonator were observed using HFSS 15.0. Based on the simulation results, the highest electric field concentration for a resonance frequency of 0.88 GHz is in the gap between the inductive arms of the ELC resonator, while the magnetic field vanishes as shown in Fig. 1(b) and Fig. 1(c). Therefore, the resonator surface with the highest electric field can be used as a sensing area to detect the permittivity of the material.

TABLE 1. Dimension of proposed resonator.

Parameter	Dimension (mm)	Parameter	Dimension (mm)
W_z	3	L_2	37
W_s	1	L_3	36
W_g	1	L_4	16
L_z	23.5	L_5	5
L_1	3	L_6	3

Furthermore, the ELC resonator can be modelled with an equivalent circuit using inductors and capacitors. The inductor represents the arm of the resonator while the capacitor represents the gap between the resonator arm and the substrate of the resonator. The values of L and C are extracted using AWR 2009 where for the arm of resonator it is represented by $L_1 = L_2 = L_3 = L_4 = 35.12$ nH while for the gap between the arm and the substrate of the sensor it is represented by $C_1 = 0.37$ pF, $C_2 = 1.04$ pF, and $C_3 = 0.273$ pF. The equivalent circuit and simulation result between the finite element model (FEM) and the equivalent circuit of the proposed resonator are shown in Fig. 2(a) and Fig. 2(b).

Based on the simulation results, it is shown that the equivalent circuit and FEM are in line where the resonance frequency of the resonator is 0.88 GHz. Furthermore, the resonance frequency of proposed resonator can be determined based on following Eq. (1):

$$f_r = \frac{1}{2\pi\sqrt{LC}} \tag{1}$$

It should be noted that the material under test (MUT) can be assumed to be capacitive load, so the interaction between resonator and the sample can be analyzed using perturbation theory as expressed in the following Eq. (2) [20]:

$$\frac{\Delta f_r}{f_r} = \frac{\int_v (\Delta\varepsilon E_1 \cdot E_0 + \Delta\mu H_1 \cdot H_0)\, dv}{\int_v \left(\varepsilon_0 |E_0|^2 + \mu_0 \cdot |H_0|^2\right) dv} \tag{2}$$

In this context, f_r denotes the resonant frequency, whereas Δf_r signifies the resonant frequency shift observed before and after loading the MUT. Changes in permittivity and permeability are denoted by $\Delta\varepsilon$ and $\Delta\mu$, respectively, while the perturbation volume is represented by v. The electric and magnetic field distributions in the absence of perturbation and with perturbation are illustrated by E_0, H_0 and E_1, H_1, respectively.

Based on Eq. (2), it is evident that variations in the permittivity or permeability of the MUT are consistent with alterations in the resonance frequency. Placement of the MUT within the sensing hotspot induces perturbations in the E-field. The interaction between the MUT and the resonator results in a shift in the resonant frequency. The relationship between the frequency shift and MUT permittivity change is denoted as frequency detection resolution (FDR). The sensor's FDR is determinable through the application of Eq. (3) [21]:

$$\text{FDR} = \frac{\Delta f}{\Delta\varepsilon_r} = \frac{(f_{\text{unloaded}} - f_{\text{loaded}})}{\varepsilon_{r(\text{MUT})} - \varepsilon_{r(\text{Reference})}}\ \text{GHz} \tag{3}$$

Generally, the reference permittivity used is a vacuum with $\varepsilon_r = 1$ as described in [3]. The normalized sensitivity (NS) can also be calculated using the equation as follows [22]:

$$\text{NS} = \frac{1}{\Delta\varepsilon_r}\left(\frac{f_{\text{unloaded}} - f_{\text{loaded}}}{f_{\text{unloaded}}}\right)\% \tag{4}$$

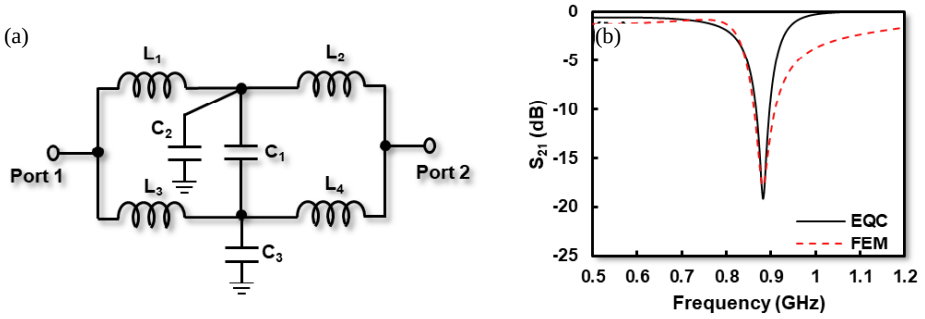

FIGURE 2. (a) Equivalent Circuit (EQC) of proposed resonator, (b) EQC vs FEM.

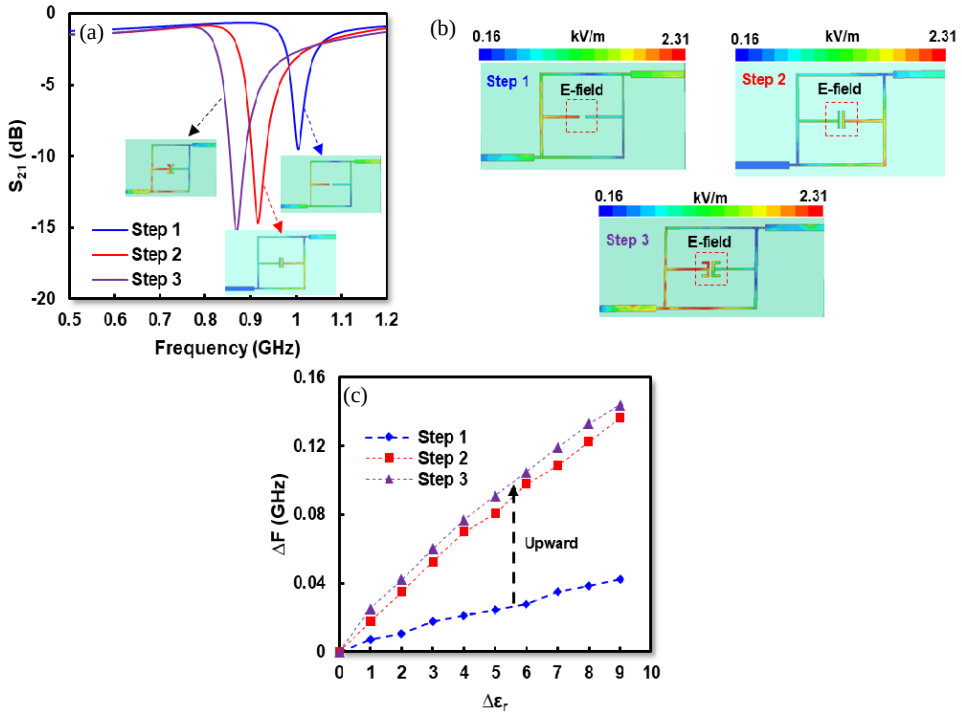

FIGURE 3. Development model of tweaking ELC resonator, (a) structure of tweaking ELC resonator, (b) E-field concentration of tweaking ELC resonator, (c) ΔF of tweaking ELC resonator.

3. SIMULATION OF PROPOSED SENSOR

The ELC resonator is developed through three stages where the location of the highest electric field is in the gap of the inductive arm of the ELC resonator. Moreover, Fig. 3(a) shows that the resonator operates at resonant frequencies of 1.00 GHz, 0.91 GHz, and 0.88 GHz for the development of the 1st step, 2nd step, and 3rd step models, respectively. Furthermore, the location of the sensing area of the ELC resonator is shown in Fig. 3(b) where the highest electric field is in the middle of the gap between the inductive arms of the resonator. Based on simulations using HFSS 15.0, the highest electric field is obtained in the structure of the 3rd step model. The interaction between the resonator and the MUT is shown in Fig. 3(c) where the ΔF with a permittivity range of 1–10 for the 1st step, 2nd step, and 3rd step models is 0.04 GHz, 0.13 GHz, and 0.14 GHz, respectively. This finding shows that the maximum ΔF is obtained in the 3rd step model.

The microwave sensor is simulated using HFSS 15.0 where the material under test (MUT) is placed in the sensing area determined based on the highest electric field concentration. The dimensions of the MUT are 10 mm × 10 mm with a thickness of 1 mm, and it is placed above the sensing area of the resonator. The correlation of the resonant frequency and permittivity from the simulation process is shown in Fig. 4(a) and Fig. 4(b).

Figure 4(a) shows that the resonant frequency of the resonator moves to a lower frequency in line with the increase in the permittivity of the MUT. Furthermore, Fig. 4(b) shows that the resonant frequency of the resonator shifts from 0.88 GHz to 0.74 GHz with $\Delta F = 0.14$ GHz for the permittivity range 1–10. These findings indicate that the permittivity of the MUT greatly influences the resonant frequency of the resonator. Furthermore, the correlation between the $\tan\delta$ of the MUT and the transmission coefficient (S_{21}) of the resonator is shown in Fig. 4(a).

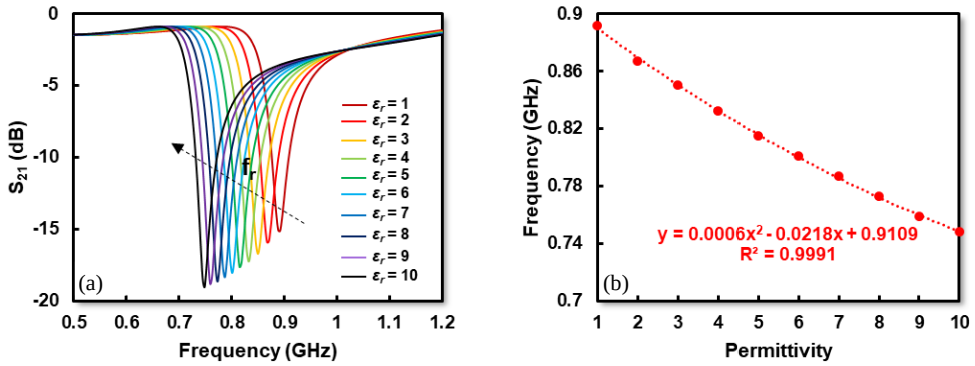

FIGURE 4. (a) Response of resonant frequency vs permittivity changes, (b) correlation between resonant frequency and permittivity.

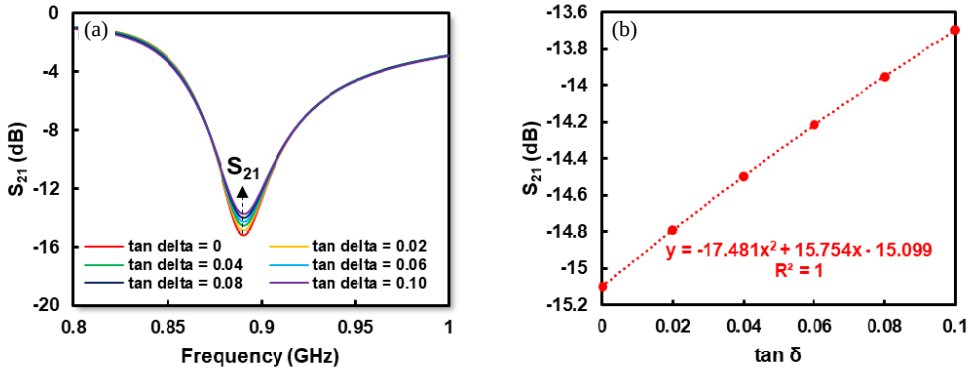

FIGURE 5. (a) Response of resonant frequency vs tanδ, (b) correlation between resonant frequency and tanδ.

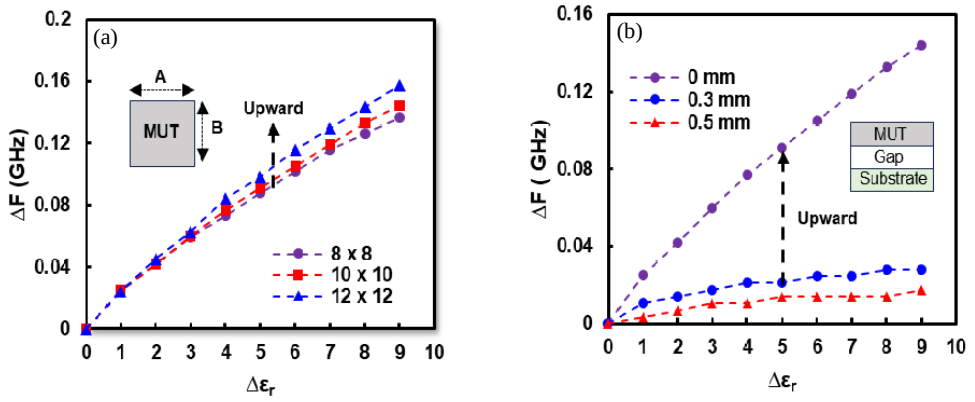

FIGURE 6. (a) ΔF of sensor based on dimension of MUT, (b) ΔF of sensor based on gap between sensor and MUT.

Furthermore, the correlation between the tan δ of the MUT and the transmission coefficient (S_{21}) of the resonator is shown in Fig. 5(a). These findings indicate that the transmission coefficient moves to low values in line with the increase in tan δ of the MUT. The transmission coefficient (S_{21}) of the resonator shifts from -15.09 dB to -13.69 dB for the tan δ of 0–0.1 as shown in Fig. 5(b).

Furthermore, the dimensions of the MUT and the air gap between the MUT and the resonator influence the performance of the sensor. Fig. 6(a) shows that the ΔF of the sensor is influenced by the dimensions of the MUT. The ΔF of the sensor in the permittivity range 1–10 with MUT dimensions of 8 mm $\times$ 8 mm, 10 mm $\times$ 10 mm, 12 mm $\times$ 12 mm and thickness of 1 mm is 0.13 GHz, 0.14 GHz, and 0.15 GHz, respectively. These findings indicate that the increase in ΔF of the sensor is in line with the increase in the dimensions of the MUT. Furthermore, the effect of the gap between the sensor and the MUT is shown in Fig. 6(b) where the ΔF of the sensor with an air gap of 0 mm, 0.3 mm, and 0.5 mm is 0.14 GHz, 0.03 GHz, and 0.02 GHz, respectively. This finding shows that the maximum ΔF is obtained when the air gap is 0 mm which means that MUT is in direct contact with the surface of the sensor.

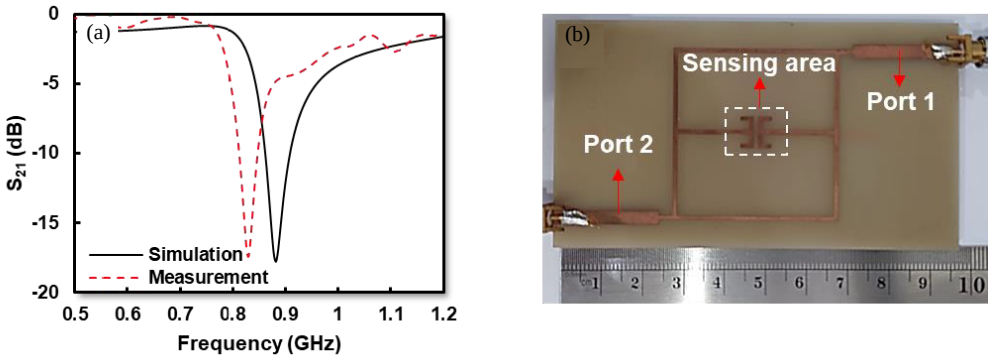

FIGURE 7. (a) Comparison simulation and measurement, (b) fabrication of proposed resonator.

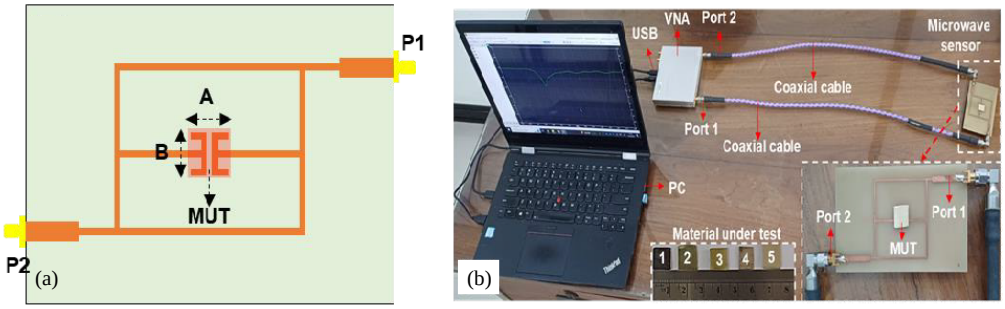

FIGURE 8. (a) Scenario of sample placement, (b) measurement setup of proposed sensor.

4. FABRICATION AND VALIDATION OF PROPOSED SENSOR

The proposed microwave sensor is fabricated using an FR-4 substrate where the ELC resonator is located on the front layer while the bottom layer functions as a ground plane with dimension of 95 mm × 42 mm with thickness of 1.6 mm. The proposed sensor consists of two input ports represented by P1 and P2 which are connected to an RP-SMA connector via a microstrip line with an impedance of 50 Ω as shown in Fig. 7(b). Validation and verification were carried out in the laboratory using a Vector Network Analyzer (VNA) with a frequency range of 0.5–1.2 GHz, sweep frequency of 0.01 GHz, and an ambient temperature of 25°C. The measurement and fabrication of the proposed sensor are shown in Fig. 7(a) and Fig. 7(b).

Figure 7(a) shows that there is a slight difference between the simulation and measurement results where the resonance frequency shifts from 0.88 GHz to 0.82 GHz. This is caused by an error during the fabrication process. Furthermore, the scenario of permittivity detection of solid material using proposed sensor has been described in Fig. 8(a) where the sample placed in the sensing area of proposed sensor with fix dimensions of 10 mm × 10 mm with thickness range of 1.58–1.6 mm represented by A and B. In this work, five types of solid materials with known permittivity in the permittivity range of 2.2–9.8 are used as MUTs with specific characteristics as shown in Table 2.

TABLE 2. Specification of MUT.

Type	Permittivity	Thickness	Tanδ
RO5880	2.2	1.58	0.0009
RO4003C	3.65	1.6	0.0027
FR4	4.3	1.6	0.0265
RO3006	6.15	1.58	0.0025
TM10i	9.8	1.58	0.002

The measurement setup for this work is shown in Fig. 8(b) where port 1 and port 2 of the sensor are connected to the VNA using a coaxial cable, while the MUT is placed above the sensing area of the sensor. The measurement results are displayed on the computer screen which is connected to the VNA using a USB cable.

Furthermore, the permittivity of the MUT is determined by observing the correlation between the permittivity and the resonant frequency of the sensor which is modelled using a polynomial equation. Based on the measurement results, the resonant frequency of the resonator experienced changes in line with increasing permittivity of the MUT as shown in Fig. 9(a). The resonant frequency of the resonator shifts to a low frequency from 0.84 GHz to 0.73 GHz for a permittivity range of 1–9.8. Additionally, the ΔF of the sensor is determined by calculating the difference between the resonant frequencies of the resonator for the lowest and highest permittivities. From the measurement results, the maximum ΔF of the proposed sensor is 0.11 GHz as shown in Fig. 9(b). Therefore, the frequency detection resolution (FDR) and normalized sensitivity (NS) of the proposed sensor can be determined based on Eq. (3) and Eq. (4) where the FDR is 0.0125 GHz and NS is 1.49%, respectively.

To determine the accuracy of the proposed sensor, the permittivity based on the measurement results is extracted using a

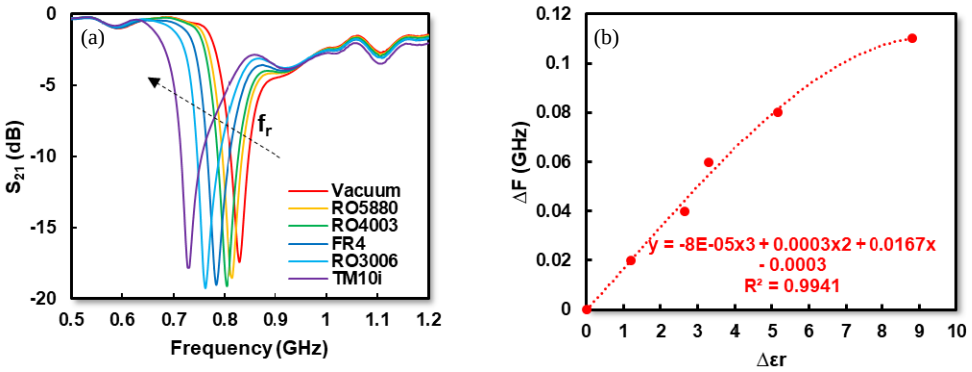

FIGURE 9. (a) Measurement of resonant frequency vs permittivity, (b) measurement of correlation between frequency vs permittivity.

TABLE 3. Comparison between permittivity from reference and calculations.

Type of MUT	ε_r reference	ε_r calculated	Error	Accuracy
Vacuum	1	0.97	2.63	97.37%
RO5880	2.2	2.33	5.84	94.16%
RO4003	3.65	3.40	6.79	93.21%
FR4	4.3	4.53	5.38	94.62%
RO3006	6.15	6.05	1.57	98.43%
TM10i	9.8	9.81	0.11	99.89%

TABLE 4. Comparison of proposed sensor with existing works.

Reference	Model	Frequency (GHz)	Band region	Low Frequency Features			Parameter	
				Lower power consumption	Reduced interference and noise	Cost-effective design	Accuracy (%)	NS (%)
[17]	U-shaped resonator	1.21 2.10	L-band	++	++	++	99.02 96.44	0.761 1.150
[23]	Omega-Shaped Resonator	1.95	L-band	++	++	++	NA	0.220
[15]	SSRR with spurlines	2.20	S-band	++	++	++	98.36	1.340
[24]	Substrate- Integrated Waveguide (SIW)	2.27	S-band	++	++	++	99.22	0.012
[18]	Substrate- Integrated Waveguide (SIW)	2.45	S-band	++	++	++	92.23	0.110
[25]	Chiral Metamaterial Sensor	4.62	C-band	+	+	+	NA	0.012
[19]	Substrate-Integrated Waveguide (SIW)	5.81	C-band	+	+	+	NA	0.140
[26]	Folded-waveguide cavities	5.84	C-band	+	+	+	NA	0.030
[16]	Aperture coupling	9.54 12.30	X-band	+	+	+	93.30	0.640
This work	Tweaking ELC resonator	0.82	UHF-band	+++	+++	+++	96.72	1.492

Notes: + bad, ++ average, and +++ good

polynomial equation and compared with the reference permittivity from the datasheet as shown in Fig. 10(a) and Fig. 10(b). The permittivity of the MUT based on the measurement results can be determined based on Eq. (5) as follows:

$$\varepsilon_{r(cal)} = -7022f_r + 169923f_r - 13646f_r + 3685.1 \quad (5)$$

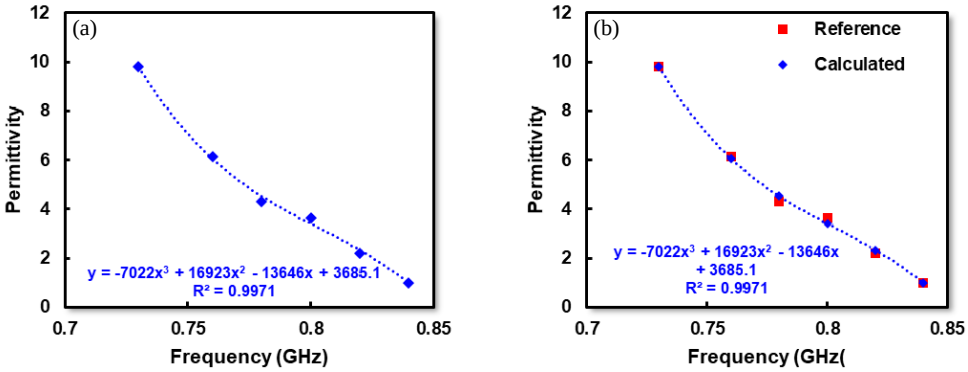

FIGURE 10. (a) Correlation between permittivity and resonant frequency, (b) comparison permittivity from reference and calculation.

where $\varepsilon_{r(cal)}$ represents the permittivity based on calculations, and f_r is the resonance frequency of the resonator. A comparison between permittivity from the datasheet and calculations is shown in Table 3.

Based on Table 3, the proposed sensor has high performance for permittivity detection with an average accuracy of 96.72% compared to the reference permittivity from the datasheet in the range from 1 to 9.8. Furthermore, to show the contribution and novelty of this work, a fair comparison with existing work is shown in Table 4.

Table 4 shows that the proposed sensor has higher normalized sensitivity than previous works. In addition, the resonant frequency proposed in previous work is in the high frequency with range of 1–12 GHz which has the potential to influence environmental interference with high cost and high-power consumption. Therefore, this work provides an excellent solution for high performance microwave sensors which operate in the UHF band with low frequency, low cost, and low power consumption compared with previous work.

5. CONCLUSION

This paper comprehensively describes a UHF-band microwave sensor for solid material characterization. The proposed microwave sensor is based on a tweaking ELC resonator operating at UHF-band with the resonant frequency of 0.82 GHz. Five types of solid materials with known permittivity were used as samples with a permittivity range of 1–9.8. Based on measurements, the proposed sensor has high performance with an average accuracy of 96.72% and a normalized sensitivity of 1.25%. Therefore, this work can be recommended for several applications such as the pharmaceutical, biomedical, and materials industries.

ACKNOWLEDGEMENT

This work was supported by Ministry of Education and Culture of the Republic of Indonesia and Institute for Research and Community Service Universitas Trisakti for fiscal years of 2024.

REFERENCES

[1] Karimi, M. A., M. Arsalan, and A. Shamim, "Multi-channel, microwave-based, compact printed sensor for simultaneous and independent level measurement of eight liquids," *IEEE Sensors Journal*, Vol. 19, No. 14, 5611–5620, 2019.

[2] Mohd Bahar, A. A., Z. Zakaria, M. K. M. Arshad, A. A. M. Isa, Y. Dasril, and R. A. Alahnomi, "Real time microwave biochemical sensor based on circular SIW approach for aqueous dielectric detection," *Scientific Reports*, Vol. 9, No. 1, 5467, 2019.

[3] Ebrahimi, A., J. Scott, and K. Ghorbani, "Differential sensors using microstrip lines loaded with two split-ring resonators," *IEEE Sensors Journal*, Vol. 18, No. 14, 5786–5793, 2018.

[4] Yeo, J. and J.-I. Lee, "High-sensitivity microwave sensor based on an interdigital-capacitor-shaped defected ground structure for permittivity characterization," *Sensors*, Vol. 19, No. 3, 498, 2019.

[5] Baghelani, M., Z. Abbasi, and M. Daneshmand, "Noncontact high sensitivity chipless tag microwave resonator for bitumen concentration measurement at high temperatures," *Fuel*, Vol. 265, 116916, 2020.

[6] Armghan, A., T. M. Alanazi, A. Altaf, and T. Haq, "Characterization of dielectric substrates using dual band microwave sensor," *IEEE Access*, Vol. 9, 62 779–62 787, 2021.

[7] Morales-Lovera, H.-N., J.-L. Olvera-Cervantes, A.-E. Perez-Ramos, A. Corona-Chavez, and C. E. Saavedra, "Microstrip sensor and methodology for the determination of complex anisotropic permittivity using perturbation techniques," *Scientific Reports*, Vol. 12, No. 1, 2205, 2022.

[8] Lobato-Morales, H., A. Corona-Chávez, J. L. Olvera-Cervantes, R. A. Chávez-Pérez, and J. L. Medina-Monroy, "Wireless sensing of complex dielectric permittivity of liquids based on the RFID," *IEEE Transactions on Microwave Theory and Techniques*, Vol. 62, No. 9, 2160–2167, 2014.

[9] Al-Behadili, A. A., I. A. Mocanu, N. Codreanu, and M. Pantazica, "Modified split ring resonators sensor for accurate complex permittivity measurements of solid dielectrics," *Sensors*, Vol. 20, No. 23, 6855, 2020.

[10] Alam, S., Z. Zakaria, I. Surjati, N. A. Shairi, M. Alaydrus, and T. Firmansyah, "Multifunctional of dual-band permittivity sensors with antenna using multicascode T-shaped resonators for simultaneous measurement of solid materials and data transfer capabilities," *Measurement*, Vol. 217, 113078, 2023.

[11] Piekarz, I., K. Wincza, S. Gruszczynski, and J. Sorocki, "Detection of methanol contamination in ethyl alcohol employing a purpose-designed high-sensitivity microwave sensor," *Measurement*, Vol. 174, 108993, 2021.

[12] Kiani, S., P. Rezaei, and M. Fakhr, "Real-time measurement of liquid permittivity through label-free meandered microwave sensor," *IETE Journal of Research*, 1–11, 2023.

[13] Alahnomi, R. A., Z. Zakaria, Z. M. Yussof, A. A. Althuwayb, A. Alhegazi, H. Alsariera, and N. A. Rahman, "Review of recent microwave planar resonator-based sensors: Techniques of complex permittivity extraction, applications, open challenges and future research directions," *Sensors*, Vol. 21, No. 7, 2267, 2021.

[14] Muñoz-Enano, J., P. Vélez, M. Gil, and F. Martín, "Planar microwave resonant sensors: A review and recent developments," *Applied Sciences*, Vol. 10, No. 7, 2615, 2020.

[15] Alahnomi, R. A., Z. Zakaria, E. Ruslan, S. R. A. Rashid, and A. A. M. Bahar, "High-Q sensor based on symmetrical split ring resonator with spurlines for solids material detection," *IEEE Sensors Journal*, Vol. 17, No. 9, 2766–2775, 2017.

[16] Behdani, M., M. M. H. Kalateh, H. Saghlatoon, J. Melzer, and R. Mirzavand, "High-resolution dielectric constant measurement using a sensor antenna with an allocated link for data transmission," *IEEE Sensors Journal*, Vol. 20, No. 24, 14 827–14 835, 2020.

[17] Alam, S., Z. Zakaria, I. Surjati, N. A. Shairi, M. Alaydrus, and T. Firmansyah, "Dual-band independent permittivity sensor using single-port with a pair of U-shaped structures for solid material detection," *IEEE Sensors Journal*, Vol. 22, No. 16, 16 111–16 119, 2022.

[18] Massoni, E., G. Siciliano, M. Bozzi, and L. Perregrini, "Enhanced cavity sensor in SIW technology for material characterization," *IEEE Microwave and Wireless Components Letters*, Vol. 28, No. 10, 948–950, 2018.

[19] Salim, A. and S. Lim, "TM02 quarter-mode substrate-integrated waveguide resonator for dual detection of chemicals," *Sensors*, Vol. 18, No. 6, 1964, 2018.

[20] Boybay, M. S. and O. M. Ramahi, "Material characterization using complementary split-ring resonators," *IEEE Transactions on Instrumentation and Measurement*, Vol. 61, No. 11, 3039–3046, 2012.

[21] Wang, C., L. Ali, F.-Y. Meng, K. K. Adhikari, Z. L. Zhou, Y. C. Wei, D. Q. Zou, and H. Yu, "High-accuracy complex permittivity characterization of solid materials using parallel interdigital capacitor-based planar microwave sensor," *IEEE Sensors Journal*, Vol. 21, No. 5, 6083–6093, 2021.

[22] Rahman, N. A., Z. Zakaria, R. A. Rahim, M. A. M. Said, A. A. M. Bahar, R. A. Alahnomi, and A. Alhegazi, "High quality factor using nested complementary split ring resonator for dielectric properties of solids sample," *The Applied Computational Electromagnetics Society Journal*, Vol. 35, No. 10, 1222–1227, 2020.

[23] Abdulkarim, Y. I., L. Deng, M. Karaaslan, *et al.*, "Novel metamaterials-based hypersensitized liquid sensor integrating omega-shaped resonator with microstrip transmission line," *Sensors*, Vol. 20, No. 3, 943, 2020.

[24] Mohd Bahar, A. A., Z. Zakaria, S. R. A. Rashid, A. A. M. Isa, and R. A. Alahnomi, "High-efficiency microwave planar resonator sensor based on bridge split ring topology," *IEEE Microwave and Wireless Components Letters*, Vol. 27, No. 6, 545–547, 2017.

[25] Bakır, M., M. Karaaslan, E. Unal, F. Karadag, F. O. Alkurt, O. Altıntaş, S. Dalgac, and C. Sabah, "Microfluidic and fuel adulteration sensing by using chiral metamaterial sensor," *Journal of the Electrochemical Society*, Vol. 165, No. 11, B475–B483, 2018.

[26] Meyne, N., G. Fuge, A.-P. Zeng, and A. F. Jacob, "Resonant microwave sensors for picoliter liquid characterization and non-destructive detection of single biological cells," *IEEE Journal of Electromagnetics, RF and Microwaves in Medicine and Biology*, Vol. 1, No. 2, 98–104, 2017.